https://doi.org/10.1130/G50489.1

Manuscript received 28 February 2022 Revised manuscript received 10 June 2022 Manuscript accepted 17 August 2022

Published online 20 October 2022

© 2022 Geological Society of America. For permission to copy, contact editing@geosociety.org

Hematite accommodated shallow, transient Pleistocene slow slip in the exhumed southern San Andreas fault system, California, USA

Alexandra A. DiMonte¹, Alexis K. Ault¹, Greg Hirth² and Kelly K. Bradbury¹

- ¹Department of Geosciences, Utah State University, Logan, Utah 84322, USA
- ²Department of Earth, Environmental and Planetary Sciences, Brown University, Providence, Rhode Island 02912, USA

ABSTRACT

Slow slip is part of the earthquake cycle, but the processes controlling this phenomenon in space and time are poorly constrained. Hematite, common in continental fault zones, exhibits unique textures and (U-Th)/He thermochronometry data patterns reflecting different slip rates. We investigated networks of small hematite-coated slip surfaces in basement fault damage of exhumed strike-slip faults that connect to the southern San Andreas fault in a flower structure in the Mecca Hills, California, USA. Scanning electron microscopy shows these millimeter-thick surfaces exhibit basal hematite injection veins and layered veinlets comprising nanoscale, high-aspect-ratio hematite plates akin to phyllosilicates. Combined microstructural and hematite (U-Th)/He data (n=64 new, 24 published individual analyses) record hematite mineralization events ca. 0.8 Ma to 0.4 Ma at <1.5 km depth. We suggest these hematite faults formed via fluid overpressure, and then hematite localized repeated subseismic slip, creating zones of shallow off-fault damage as far as 4 km orthogonal to the trace of the southern San Andreas fault. Distributed hematite slip surfaces develop by, and then accommodate, transient slow slip, potentially dampening or distributing earthquake energy in shallow continental faults.

INTRODUCTION

Exhumed fault rocks record time-integrated thermochemical and mechanical signatures of past deformation processes that also currently operate at depth over repeated earthquake cycles. Minerals and slip-surface textures may generate rheological contrasts that promote different slip behaviors (Collettini et al., 2009; Williams et al., 2021). In the shallow portion of continental faults, hematite is common and forms from interactions of oxidizing groundwater with Fe-rich minerals. Hematite textures and (U-Th)/He (hematite He) thermochronometry can document the timing, temperatures, depths, and/or rates of fault slip (Ault, 2020). Recent work from natural and experimental hematite faults shows clear evidence for earthquakes (McDermott et al., 2017; Ault et al., 2019; Calzolari et al., 2020). However, other observations suggest hematite deforms subseismically (Moser et al., 2017; McDermott et al., 2021), implying hematite may accommodate a range of slip behaviors.

Fault slip is a continuum from earthquake to aseismic slip (Jolivet and Frank, 2020). This includes seismically and geodetically observed low- (and very low-) frequency earthquakes, tremor, slow-slip events, and creep events (Shelly et al., 2006; Peng and Gomberg, 2010; Beroza and Ide, 2011). We use slow slip as a general term for the release of elastic energy along faults at rates slow enough that radiated energy is not detected (Bürgmann, 2018; Jolivet and Frank, 2020). The mechanisms that cause slow slip are complex, and may include mechanical effects of increased pore-fluid pressure or heterogeneous frictional, lithologic, or geometric fault properties (McCaffrey et al., 2008; Wei et al., 2013; French and Condit, 2019; Ikari, 2019). Accurate models of slow slip integrate geophysical and geologic data that inform earthquake hazards and require direct observations of fault zones that experience limited overprinting deformation.

Along the southernmost segment of the San Andreas fault (SAF) system (California, USA), a series of oblique strike-slip faults in

the Mecca Hills connect to the southern SAF at depth in a positive flower structure (Sylvester and Smith, 1976; Fuis et al., 2017). Geophysical data show recent triggered and spontaneous shallow creep events along the southern SAF and other minor structures in the area (Allen et al., 1972; Lindsey et al., 2014; Tymofyeyeva et al., 2019; Parker et al., 2021). Prior work revealed hematite-coated slip surfaces in some basement fault zones in the Mecca Hills (Moser et al., 2017). Limited hematite He analyses identified Pleistocene hematite mineralization events at \sim 1–2 km depth (Moser et al., 2017), placing these surfaces at the target depth range to evaluate whether they accommodated shallow slow slip in the past. Here we expand this Mecca Hills hematite He data set and integrate new field and microstructural results to document where, when, and how hematite fault damage forms and deforms, with implications for how deformation occurs at depth today in the southern SAF system.

BASEMENT-HOSTED FAULT DAMAGE IN THE MECCA HILLS

Transpression on the SAF and other related faults initiated in the Pliocene, exhumed Precambrian crystalline basement and Orocopia Schist in the Mecca Hills, and formed adjacent sedimentary basins (Sylvester and Smith, 1976; Fattaruso et al., 2014; McNabb et al., 2017; Moser et al., 2017; Bergh et al., 2019; Spotila et al., 2020). Oblique strike-slip faults cut basement and Pliocene–Pleistocene sedimentary rocks, delineating separate fault blocks (Fig. 1; Sylvester and Smith, 1976). Incised canyons expose fault zones <1 km wide, including the Painted Canyon fault (PCF) and Platform fault (PF), that bound the Platform block (Sylvester and Smith, 1976). We identified a map-scale,

CITATION: DiMonte, A.A., Ault, A.K., Hirth, G., and Bradbury, K.K., 2022, Hematite accommodated shallow, transient Pleistocene slow slip in the exhumed southern San Andreas fault system, California, USA: Geology, v. XX, p. , https://doi.org/10.1130/G50489.1

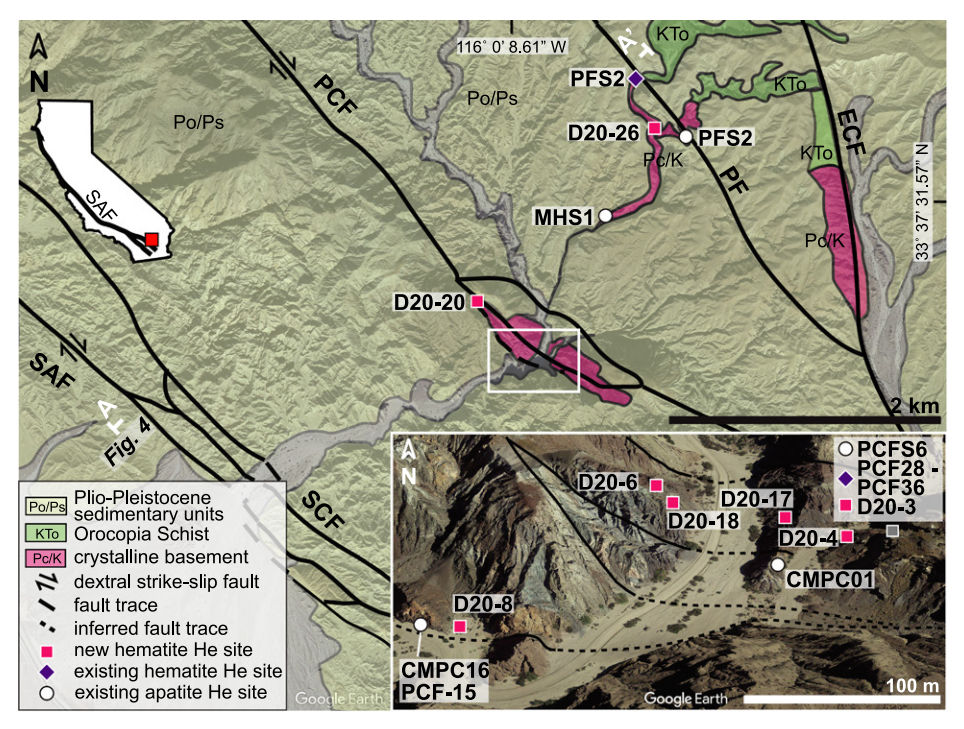


Figure 1. Simplified geologic map of the Mecca Hills, California (USA), with site locations, modified from Fattaruso et al. (2014), McNabb et al. (2017), and Moser et al. (2017). Previously published hematite He (Moser et al., 2017) and apatite He (Moser et al., 2017; Spotila et al., 2020) are shown. SAF—San Andreas fault; SCF—Skeleton Canyon fault; PCF—Painted Canyon fault; PF—Platform fault; ECF—Eagle Canyon fault; A-A′—line of cross section shown in Figure 4A. White box shows Google Earth™ inset location with site details.

low-angle normal fault in the Platform block that offsets different basement rock types. This fault does not deform the overlying sedimentary rock, and thus initial faulting predates this deposition (Fig. S1 in the Supplemental Material¹).

Fe-oxide-coated slip surfaces are ubiquitous in basement damage zones of the PCF and PF and are locally observed in the Platform block. We focus on pure hematite surfaces amenable to (U-Th)/He analysis, which occur as networks of minor (1 cm2 to 1000 cm2 surface area) faults cutting chlorite-rich schistose gneiss and epidote-rich granite (Figs. 1 and 2A; Table S1; Figs. S2 and S3). These dominantly northnorthwest- and northeast-striking surfaces are metallic, blue-gray, and curviplanar, with linear and/or curved slickenline orientations indicating oblique and dip slip with millimeter-scale offset. Newly observed mixed hematite-clay slip surfaces occur within and adjacent to layered clay gouge zones of map-scale faults.

MICROSTRUCTURAL CHARACTERIZATION

Scanning electron microscopy (SEM) with energy dispersive X-ray spectroscopy (EDS) was used to characterize 50-µm- to 2-mm-thick fault surfaces (n = 10) with nanometer-scale hematite plates that appear opaque in thin section (see the Supplemental Material for details; Fig. 2; Fig. S4). EDS data show some surfaces comprise interlayered and/or cross-cutting hematite veins with calcite and phyllosilicate veins (Fig. 2B). A subset of surfaces have cataclasite with a hematite matrix and clasts of host rock and/or reworked clasts of secondary calcite, phyllosilicate, or hematite veins (Fig. 2C). Foliated hematite locally exhibits S-C fabrics, hematite-tailed clasts, and hematite "fish", analogous to mica fish (Fig. 2F; Fig. S5). Some surfaces display \sim 10–100- μ m-wide, \sim 100- μ m- to 1-mm-long hematite-filled injection veins into host rock or calcite oriented perpendicular to the fault surface (Fig. 2D; Fig. S5).

Foliated, high-aspect-ratio hematite platelets are planar or cuspate in cross section with smooth or serrated grain boundaries (Fig. 2G; Fig. S6). Some surfaces also exhibit euhedral, hexagonal plates with equant c-axis-perpendicular cross sections (Fig. 2E; Fig. S6). For aliquots analyzed for thermochronometry, we quantified hematite plate-width distributions (n = 1567) from SEM images because this dimension is the minimum He diffusion domain length scale

(see the Supplemental Material). Plate-width measurements display a left-skewed normal distribution of 12–87 nm with a mean of 31 nm (Fig. S7); plate lengths are $\sim\!\!200$ nm to 1 μm . Observed phyllosilicates exhibit similar dimensions (Figs. S5 and S6).

HEMATITE (U-Th)/He DATA

Hematite aliquots were analyzed for He, U, and Th content at the Arizona Radiogenic Helium Dating Laboratory at the University of Arizona (Tucson, Arizona, USA) using apatite lasing temperatures (to prevent U and Th volatilization) and modified zircon dissolution procedures (see the Supplemental Material for analytical details). We present 64 new individual hematite He dates from 17 samples on 15 fault surfaces collected from eight sites (Table S2; Figs. S3 and S8) and combine these data with results previously reported by Moser et al. (2017; 24 aliquots from five surfaces; Fig. 1). We report mean dates $\pm 1\sigma$ standard deviation for all samples because they yield <15% standard deviation, except for two samples at site D20-6 (with a combined 26% standard deviation), where we report the range of individual aliquot dates with their 2σ analytical uncertainty (cf. Flowers and Kelley, 2011). We do not apply an alpha (α)-ejection correction to individual dates because α-ejection from one crystal is balanced by He implantation from another crystal in dense polycrystalline material, and \sim 75–200- μ m-thick aliquots were extracted from slip surfaces that developed within larger hematite veins. Consideration of α -ejection from aliquot margins would at most increase dates by 12% (see the Supplemental Material). For samples with dates <1 Ma, variable [234 U/ 238 U] and [230 Th/ 238 U] activity ratios may cause <15% error on individual analyses, within the standard deviation for most samples (cf. Farley et al., 2002; see the Supplemental Material).

We delineate four hematite He sample groups by structural position along a southwest-northeast transect: (1) west of the main PCF near a faulted basement-sedimentary rock nonconformity, (2) within the voluminous PCF zone, (3) near the low-angle normal fault in the Platform block, and (4) near the PF (Fig. 3). Mean dates from samples in group 1 are 0.79 ± 0.01 Ma and 0.70 ± 0.09 Ma, those in group 2 range from 0.71 ± 0.03 Ma to 0.38 ± 0.01 Ma, those in group 3 are 0.42 ± 0.05 Ma and 0.36 ± 0.02 Ma, and those in group 4 are 0.63 ± 0.09 Ma (Fig. 3). Individual dates from site D20-6 in group 2 range from 2.2 ± 0.1 Ma to 0.99 ± 0.04 Ma.

SHALLOW PLEISTOCENE HEMATITE PRECIPITATION

Polycrystalline hematite has a (U-Th)/He closure temperature (T_c) of \sim 25–250 °C (Farley, 2018) that is controlled by the grain-size

¹Supplemental Material. Method details for SEM and grain-size analyses, hematite (U-Th)/He analyses, alpha-ejection correction derivation and calculations, as well as a discussion of data outliers and disequilibrium; and three tables and 11 additional figures including field, sample, and aliquot photographs; SEM images; schematic for alpha-ejection calculation; and additional hematite (U-Th)/He data plots. Please visit https://doi.org/10.1130/GEOL.S.21183715 to access the supplemental material, and contact editing@geosociety.org with any questions.

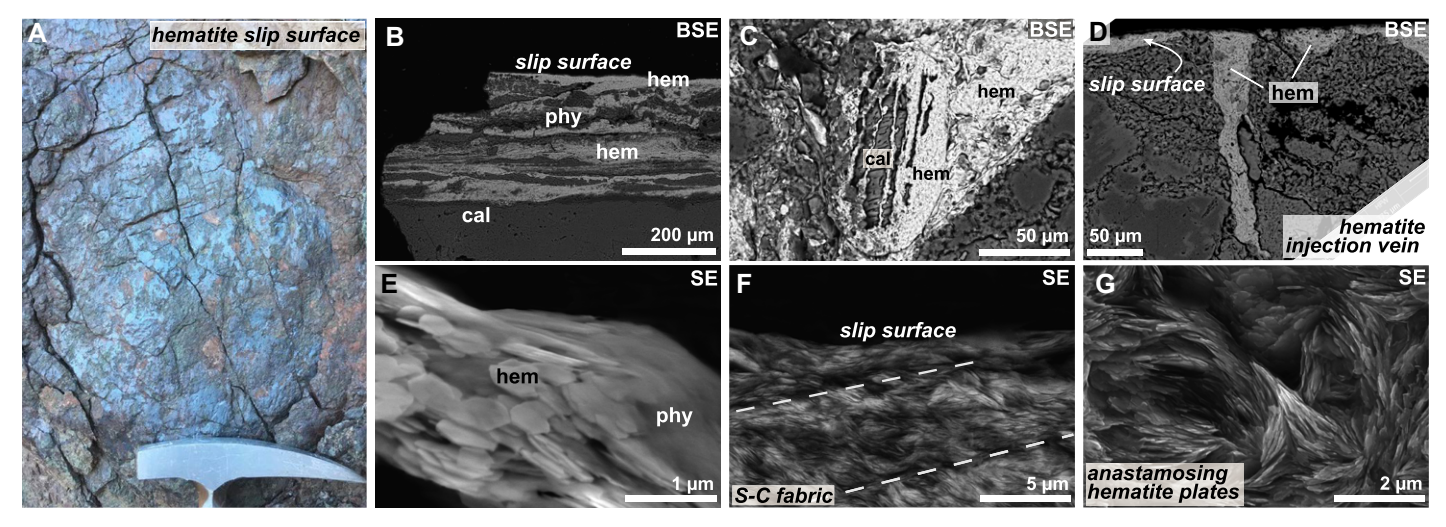


Figure 2. (A) Hematite slip surfaces in the Painted Canyon fault (Mecca Hills, California, USA). (B–D) Backscatter electron (BSE) images of slip surface with interlayered hematite (hem), phyllosilicates (phy), and calcite (cal) (B); reworked clast (C); and hematite injection vein (D). (E–G) Secondary electron (SE) images of euhedral hematite plates and phyllosilicates (E); hematite S-C fabric (F), and anastomosing hematite plates (G).

distribution. Because hematite can precipitate at temperatures above or below its T_c , we interpret the significance of our hematite He data using T_c estimates from our plate half-width distributions and ambient thermal conditions constrained by adjacent basement apatite (U-Th)/He (apatite He) thermochronometry. Assuming the diffusion kinetics of Farley (2018), a spherical geometry that yields a conservative lower T_c (compared to plane-sheet geometry), and 10 °C/m.y. cooling rate, calculated hematite He T_c values are ~ 60 – 72 °C (Fig. S7). This T_c range overlaps with that of the apatite He system (Flowers et al., 2009), so dates from each system may be directly compared (Fig. 3). Individual ca. 1.6-0.8 Ma apatite He dates across the Platform block record rapid exhumation through < 1.5 km depth at that time (Moser et al., 2017; Spotila et al., 2020). Outside the Platform block, apatite He dates are ca. 18–3 Ma, implying slower and/or a lower magnitude of exhumation (Fig. 3).

Across our transect, most (91%) individual hematite He dates are younger than structurally adjacent apatite He dates (Fig. 3) despite similar calculated $T_{\rm c}$ for all hematite aliquots and between the hematite He and apatite He systems. These patterns indicate mean hematite He dates from these samples do not record ambient cooling and instead record hematite formation from ca. 0.8 Ma to ca. 0.4 Ma at <1.5 km depth. Consideration of the maximum aliquot α -ejection correction factor or disequilibrium effects does not change these interpretations. Individual hematite He dates from site D20-6

(group 2) overlap with nearby apatite He dates; these hematite He results reflect cooling due to exhumation, with a minimum formation age of ca. 2.2 Ma.

We interpret that mean hematite He dates record episodic mineralization events because variation in mean dates among samples (~0.43 m.y.) exceeds the maximum intrasample data scatter (~0.26 m.y.). Intrasample scatter may reflect that aliquots capture multiple Pleistocene hematite generations (i.e., mixed ages). Within the PCF (group 2), mean dates from different slip surfaces within a site show broadly contemporaneous hematite formation (e.g., site D20-4) and distinct periods of mineralization (e.g., site D20-3/PCF28-PCF36; Fig. 3; Table S2). Group 3 hematite He dates are from minor

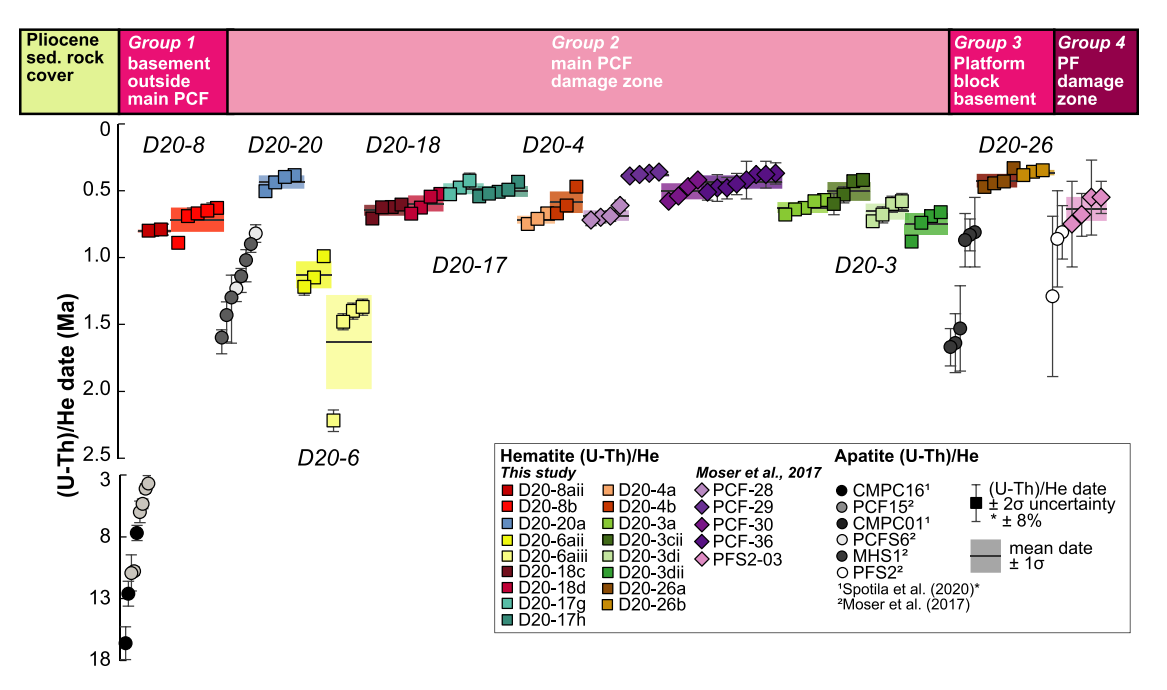


Figure 3. Individual hematite (U-Th)/He dates +2₀ analytical uncertainty. x-axis is position (not to scale) along the southwest-northeast transect; top bar is the date group and structural context. New site labels are shown in italics. Squares (this study) and diamonds (Moser et al., 2017) are colored by site; shades are different samples; sample mean + standard deviation is shown. Comparison apatite He dates, circles (Moser et al., 2017; Spotila et al., 2020), for each group are plotted to the left of hematite He dates. sed.—sedimentary; PCF—Painted Canyon fault; PF-Platform fault.

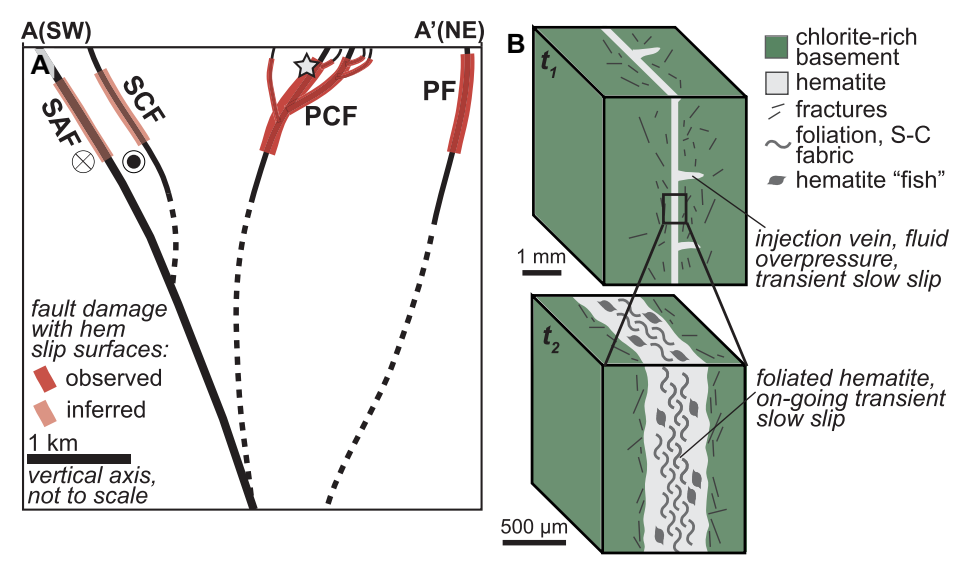


Figure 4. (A) Schematic A-A' cross section of the San Andreas fault system through the Mecca Hills (see Fig. 1 for location). Location of hematite (hem) fault damage is in red; star is an example location of B. SAF—San Andreas fault; SCF—Skeleton Canyon fault; PCF—Painted Canyon fault; PF—Platform fault. (B) Simplified block diagrams showing textural evolution of an individual hematite surface with initial precipitation (time t_1) and repeated slow slip (t_2).

slip surfaces in the damage zone of the lowangle fault within the Platform block that likely predates the SAF. Collectively, these hematite data patterns support the episodic creation and reactivation of Pleistocene hematite fault damage of larger structures linked to or not associated with the SAF.

REPEATED SLOW SLIP ON HEMATITE SLIP SURFACES

We suggest injection veins at the base of some slip surfaces reflect initial hematite precipitation during transient fluid overpressure events. Along other slip surfaces, fluid-rock interaction, including with lower-permeability clay minerals, mobilized Fe and precipitated hematite along precursor grain interfaces and in veins. Interlayered and cross-cutting hematite and calcite veins, as well as clasts of older hematite veins, indicate repeated and episodic hematite precipitation on individual slip surfaces. Hematite textures, such as S-C fabrics, demonstrate ongoing slip occurred on these surfaces following hematite growth (Fig. 2).

Hematite grain morphologies along slip surfaces are distinct from polygonal or sintered grains associated with coseismic friction-generated heat (Ault et al., 2019; Calzolari et al., 2020) or comminuted and recrystallized particles formed during propagation of seismic slip at shallow depths (Taylor et al., 2021) documented at other locations, indicating our observed textures did not form during seismic events. Our observed hematite plates have a similar aspect ratio to phyllosilicate sheets. The platy structure and crystal-bound water in phyllosilicates contribute to a low coefficient of friction and velocity-strengthening behavior

that promote stable sliding (Moore and Lockner, 2004; Collettini et al., 2009; French et al., 2015). Phyllosilicate-rich rocks can produce transient slow-slip events in the lab (Ikari, 2019). Although hematite does not contain crystal-bound water, experimental data (Calzolari et al., 2020) reveal its coefficient of friction may be comparable to that of phyllosilicates, suggesting similar frictional behavior.

Preserved plates, homogenous grain-size distributions, and foliated textures (Fig. 2) show hematite did not experience post-formation comminution and instead deformed by interplate sliding. Reproducible intrasample hematite He dates record hematite growth and indicate that repeated reactivation of these surfaces occurred at slip rates slow enough to not induce post-formation He loss. These observations imply hematite formed and continued to deform by slow slip.

GEOLOGIC CONTROLS ON SHALLOW TRANSIENT SLOW SLIP

Hematite He thermochronometry lacks the temporal resolution to characterize the time scale(s) of a slow-slip (or earthquake) cycle. However, these data bracket episodes of past fault damage creation and, when integrated with microstructures, inform transient aseismic slip processes, such as slow-slip events, that may occur at depth today along shallow continental faults including the SAF. In the Mecca Hills, we interpret that networks of small hematite slip surfaces, each with millimeters of cumulative offset, in damage zones of the PCF and PF and structures within the Platform block developed by repeated, transient slow slip at <1.5 km depth between ca. 0.8 Ma and 0.4 Ma. Transient slow slip was subsequently localized on these surfaces, likely even after ca. 0.4 Ma. Hematite fault damage is preserved as far as 4 km perpendicular to the main trace of the southern SAF, revealing the spatial scales of past transient slow slip in off-fault damage of the SAF system (Fig. 4A).

Development of hematite fault damage influences shallow fault rheology that may contribute to slow slip at depth in the southern SAF system (Fig. 4) and other continental faults worldwide (e.g., Calzolari et al., 2018; McDermott et al., 2021). We suggest that hematite damage initially forms by pore-fluid overpressure and fluidrock interaction reflecting transient slow slip (Fig. 4B). Once formed, slip-surface networks of anisotropic, foliated hematite (Fig. 4B), which may be weaker than the surrounding basement rock, continue to deform by transient slow slip. Observations from the shallow rock record reveal hematite, like phyllosilicates, may play a role in accommodating the aseismic propagation of transient or triggered slow slip, potentially distributing earthquake energy or facilitating arrest of earthquakes in the shallowest crust.

ACKNOWLEDGMENTS

This work is supported by U.S. National Science Foundation (EAR-2039727) and Southern California Earthquake Center (SCEC; 21068) grants to Ault and Hirth; and by Geological Society of America and Utah State University Graduate Student Research Grants to DiMonte. This is SCEC contribution no. 12615. We thank Pete Reiners, Uttam Chowdhury, and Fen-Ann Shen for analytical assistance; Roland Bürgmann for helpful discussions; and Matt Ikari and two anonymous reviewers for excellent feedback that improved the manuscript.

REFERENCES CITED

Allen, C.R., Wyss, M., Brune, J.N., Grantz, A., and Wallace, R.E., 1972, Displacements on the Imperial, Superstition Hills, and San Andreas faults triggered by the Borrego Mountain earthquake, in The Borrego Mountain Earthquake of April 9, 1968: U.S. Geological Survey Professional Paper 787, p. 87–104, https://doi.org/10.3133/pp787.

Ault, A.K., 2020, Hematite fault rock thermochronometry and textures inform fault zone processes: Journal of Structural Geology, v. 133, 104002, https://doi.org/10.1016/j.jsg.2020.104002.

Ault, A.K., Jensen, J.L., McDermott, R.G., Shen, F.-A., and Van Devener, B.R., 2019, Nanoscale evidence for temperature-induced transient rheology and postseismic fault healing: Geology, v. 47, p. 1203–1207, https://doi.org/10.1130/G46317.1.

Bergh, S.G., Sylvester, A.G., Damte, A., and Indrevær, K., 2019, Polyphase kinematic history of transpression along the Mecca Hills segment of the San Andreas fault, southern California: Geosphere, v. 15, p. 901–934, https://doi.org/10.1130/GES02027.1.

Beroza, G.C., and Ide, S., 2011, Slow earthquakes and nonvolcanic tremor: Annual Review of Earth and Planetary Sciences, v. 39, p. 271–296, https:// doi.org/10.1146/annurev-earth-040809-152531.

Bürgmann, R., 2018, The geophysics, geology and mechanics of slow fault slip: Earth and Planetary Science Letters, v. 495, p. 112–134, https://doi.org/10.1016/j.epsl.2018.04.062.

Calzolari, G., Rossetti, F., Ault, A.K., Lucci, F., Olivetti, V., and Nozaem, R., 2018, Hematite (U-Th)/He thermochronometry constrains strike-slip faulting

- on the Kuh-e-Faghan fault, central Iran: Tectonophysics, v. 728–729, p. 41–54, https://doi.org/10.1016/j.tecto.2018.01.023.
- Calzolari, G., Ault, A.K., Hirth, G., and McDermott, R.G., 2020, Hematite (U-Th)/He thermochronometry detects asperity flash heating during laboratory earthquakes: Geology, v. 48, p. 514– 518, https://doi.org/10.1130/G46965.1.
- Collettini, C., Niemeijer, A., Viti, C., and Marone, C., 2009, Fault zone fabric and fault weakness: Nature, v. 462, p. 907–910, https://doi.org/10.1038/nature08585.
- Farley, K.A., 2018, Helium diffusion parameters of hematite from a single-diffusion-domain crystal: Geochimica et Cosmochimica Acta, v. 231, p. 117–129, https://doi.org/10.1016/j.gca.2018 04 005
- Farley, K.A., Kohn, B.P., and Pillans, B., 2002, The effects of secular disequilibrium on (U-Th)/He systematics and dating of Quaternary volcanic zircon and apatite: Earth and Planetary Science Letters, v. 201, p. 117–125, https://doi.org/10.1016/S0012-821X(02)00659-3.
- Fattaruso, L.A., Cooke, M.L., and Dorsey, R.J., 2014, Sensitivity of uplift patterns to dip of the San Andreas fault in the Coachella Valley, California: Geosphere, v. 10, p. 1235–1246, https://doi.org/10.1130/GES01050.1.
- Flowers, R.M., and Kelley, S.A., 2011, Interpreting data dispersion and "inverted" dates in apatite (U-Th)/He and fission-track datasets: An example from the US midcontinent: Geochimica et Cosmochimica Acta, v. 75, p. 5169–5186, https://doi.org/10.1016/j.gca.2011.06.016.
- Flowers, R.M., Ketcham, R.A., Shuster, D.L., and Farley, K.A., 2009, Apatite (U-Th)/He thermochronometry using a radiation damage accumulation and annealing model: Geochimica et Cosmochimica Acta, v. 73, p. 2347–2365, https://doi.org/10.1016/j.gca.2009.01.015.
- French, M.E., and Condit, C.B., 2019, Slip partitioning along an idealized subduction plate boundary at deep slow slip conditions: Earth and Planetary Science Letters, v. 528, 115828, https://doi.org/10.1016/j.epsl.2019.115828.
- French, M.E., Chester, F.M., and Chester, J.S., 2015, Micromechanisms of creep in clay-rich gouge from the Central Deforming Zone of the San Andreas Fault: Journal of Geophysical Research: Solid Earth, v. 120, p. 827–849, https://doi.org/10.1002/2014JB011496.
- Fuis, G.S., et al., 2017, Subsurface geometry of the San Andreas fault in southern California: Results from the Salton Seismic Imaging Project (SSIP) and strong ground motion expectations: Bulletin

- of the Seismological Society of America, v. 107, p. 1642–1662, https://doi.org/10.1785/0120160309.
- Ikari, M.J., 2019, Laboratory slow slip events in natural geological materials: Geophysical Journal International, v. 218, p. 354–387, https://doi.org/10.1093/gji/ggz143.
- Jolivet, R., and Frank, W.B., 2020, The transient and intermittent nature of slow slip: AGU Advances, v. 1, e2019AV000126, https://doi.org/10.1029/2019AV000126.
- Lindsey, E.O., Fialko, Y., Bock, Y., Sandwell, D.T., and Bilham, R., 2014, Localized and distributed creep along the southern San Andreas Fault: Journal of Geophysical Research: Solid Earth, v. 119, p. 7909– 7922, https://doi.org/10.1002/2014JB011275.
- McCaffrey, R., Wallace, L.M., and Beavan, J., 2008, Slow slip and frictional transition at low temperature at the Hikurangi subduction zone: Nature Geoscience, v. 1, p. 316–320, https://doi.org/10.1038/ngeo178.
- McDermott, R.G., Ault, A.K., Evans, J.P., and Reiners, P.W., 2017, Thermochronometric and textural evidence for seismicity via asperity flash heating on exhumed hematite fault mirrors, Wasatch fault zone, UT, USA: Earth and Planetary Science Letters, v. 471, p. 85–93, https://doi.org/10.1016/j.eps1.2017.04.020.
- McDermott, R.G., Ault, A.K., and Caine, J.S., 2021, Dating fault damage along the eastern Denali fault zone with hematite (U-Th)/He thermochronometry: Earth and Planetary Science Letters, v. 563, 116872, https://doi.org/10.1016/j.epsl.2021.116872.
- McNabb, J.C., Dorsey, R.J., Housen, B.A., Dimitroff, C.W., and Messé, G.T., 2017, Stratigraphic record of Pliocene-Pleistocene basin evolution and deformation within the southern San Andreas fault zone, Mecca Hills, California: Tectonophysics, v. 719–720, p. 66–85, https://doi.org/10.1016/j .tecto.2017.03.021.
- Moore, D.E., and Lockner, D.A., 2004, Crystallographic controls on the frictional behavior of dry and water-saturated sheet structure minerals: Journal of Geophysical Research, v. 109, B03401, https://doi.org/10.1029/2003JB002582.
- Moser, A.C., Evans, J.P., Ault, A.K., Janecke, S.U., and Bradbury, K.K., 2017, (U-Th)/He thermochronometry reveals Pleistocene punctuated deformation and synkinematic hematite mineralization in the Mecca Hills, southernmost San Andreas Fault zone: Earth and Planetary Science Letters, v. 476, p. 87–99, https://doi.org/10.1016/j.epsl.2017.07.039.
- Parker, J., Donnellan, A., Bilham, R., Ludwig, L.G., Wang, J., Pierce, M., Mowery, N., and Jänecke,

- S., 2021, Buried aseismic slip and off-fault deformation on the southernmost San Andreas fault triggered by the 2010 El Mayor Cucapah earthquake revealed by UAVSAR: Earth and Space Science, v. 8, e2021EA001682, https://doi.org/10.1029/2021EA001682.
- Peng, Z.G., and Gomberg, J., 2010, An integrated perspective of the continuum between earthquakes and slow-slip phenomena: Nature Geoscience, v. 3, p. 599–607, https://doi.org/10.1038/ngeo940.
- Shelly, D.R., Beroza, G.C., Ide, S., and Nakamula, S., 2006, Low-frequency earthquakes in Shikoku, Japan, and their relationship to episodic tremor and slip: Nature, v. 442, p. 188–191, https://doi.org/10.1038/nature04931.
- Spotila, J.A., Mason, C.C., Valentino, J.D., and Cochran, W.J., 2020, Constraints on rock uplift in the eastern Transverse Ranges and northern Peninsular Ranges and implications for kinematics of the San Andreas fault in the Coachella Valley, California, USA: Geosphere, v. 16, p. 723–750, https://doi.org/10.1130/GES02160.1.
- Sylvester, A.G., and Smith, R.R., 1976, Tectonic transpression and basement-controlled deformation in San Andreas fault zone, Salton Trough, California: American Association of Petroleum Geologists Bulletin, v. 60, p. 2081–2102, https://doi.org/10.1306/C1EA3A73-16C9-11D7-8645000102C1865D.
- Taylor, M.P., Ault, A.K., Odlum, M.L., and Newell, D.L., 2021, Shallow rupture propagation of Pleistocene earthquakes along the Hurricane fault, UT, revealed by hematite (U-Th)/He thermochronometry and textures: Geophysical Research Letters, v. 48, e2021GL094379, https://doi.org/10.1029 /2021GL094379.
- Tymofyeyeva, E., et al., 2019, Slow slip event on the southern San Andreas fault triggered by the 2017 M_w 8.2 Chiapas (Mexico) earthquake: Journal of Geophysical Research: Solid Earth, v. 124, p. 9956–9975, https://doi.org/10.1029/2018JB016765.
- Wei, M., Kaneko, Y., Liu, Y.J., and McGuire, J.J., 2013, Episodic fault creep events in California controlled by shallow frictional heterogeneity: Nature Geoscience, v. 6, p. 566–570, https://doi.org/10.1038/ngeo1835.
- Williams, R.T., Rowe, C.D., Okamoto, K., Savage, H.M., and Eves, E., 2021, How fault rocks form and evolve in the shallow San Andreas fault: Geochemistry Geophysics Geosystems, v. 22, e2021GC010092, https://doi.org/10.1029/2021GC010092.

Printed in USA